Deterministic encapsulation of single cells in thin tunable microgels for niche modelling and therapeutic delivery

Angelo S. Mao[1,2†], Jae-Won Shin[1,2,3†], Stefanie Utech[2], Huanan Wang[2,4,5], Oktay Uzun[1,2], Weiwei Li[1,2], Madeline Cooper[2], Yuebi Hu[2], Liyuan Zhang[2,4], David A. Weitz[1,2,4] and David J. Mooney[1,2]*

Existing techniques to encapsulate cells into microscale hydrogels generally yield high polymer-to-cell ratios and lack control over the hydrogel's mechanical properties[1]. Here, we report a microfluidic-based method for encapsulating single cells in an approximately six-micrometre layer of alginate that increases the proportion of cell-containing microgels by a factor of ten, with encapsulation efficiencies over 90%. We show that *in vitro* cell viability was maintained over a three-day period, that the microgels are mechanically tractable, and that, for microscale cell assemblages of encapsulated marrow stromal cells cultured in microwells, osteogenic differentiation of encapsulated cells depends on gel stiffness and cell density. We also show that intravenous injection of singly encapsulated marrow stromal cells into mice delays clearance kinetics and sustains donor-derived soluble factors *in vivo*. The encapsulation of single cells in tunable hydrogels should find use in a variety of tissue engineering and regenerative medicine applications.

Encapsulation of single cells in a thin hydrogel layer could lead to advances in a variety of fields by offering precise microscale control in assembly of complex tissue mimics and programming *in vivo* delivery of cells via different routes of administration. Advances in microfluidics and surfactant chemistry have enabled encapsulation of cells in microscale hydrogels[1], but current microgels are generally much larger than the cells they encapsulate[1–4], and high cell densities, resulting in multiple cells per microgel[5], are required to increase the fraction of microgels containing cells. Production of a pure population of cell-encapsulation microgels without secondary sorting steps[6] would potentially improve workflow in pre-clinical and clinical settings. Recent approaches that use synchronization between emulsion formation and ordered cell flow to achieve high yield[7,8] have yet to be tested in the context of hydrogel encapsulation. Although cells have been coated in polymer layers[9–12], many of these approaches chemically modify cell surface components, and how this influences cellular functions is unclear; thus far, there have been no reports that demonstrate *in vitro* differentiation or *in vivo* delivery of singly coated stem cells. Moreover, although providing the appropriate matrix cues has been shown to be a potent method for producing desired biological phenomena of encapsulated cells[13], there has been little work to control local properties of hydrogels at the single-cell level to influence the biological functions of encapsulated cells, either *in vitro* or *in vivo*.

Here, we fabricated a pure population of cell-containing microgels using alginate, a biocompatible polymer with a gentle mode of crosslinking mediated by soluble calcium[14], by first exposing cells to a suspension of calcium carbonate nanoparticles, which allowed passive adsorption to the cell surface in a concentration-dependent manner (Fig. 1a and Supplementary Fig. 1a). Adsorption was observed on all cell types tested, although different cell types appeared to have different propensities for adsorbing nanoparticles, presumably reflecting differences in membrane composition and cell size (Supplementary Table 1). After excess nanoparticles were washed away, cells were combined with soluble alginate polymer, and a cross-junction microfluidic device[15] was used to generate a water-in-oil emulsion[16]; acetic acid in the oil phase mediated calcium release from nanoparticles (Supplementary Fig. 1b, see Methods). The fraction of microgels containing cells (yield) resulting from this pre-coating step was dramatically increased in comparison to direct injection without pre-coating. As encapsulation of cells and particles into picolitre droplets follows a Poisson process[5], the Poisson distributions produced from experimentally calculated λ were calculated and graphed for murine marrow stromal cells (mMSCs) and murine pre-adipocyte cells (OP9s)[17,18] (Fig. 1b,c). The probability density functions of cell-encapsulating microgels both with and without the pre-coating step generally retain the shape of a Poisson distribution, except with a rightward translation after nanoparticle pre-coating. Encapsulation yields of both pre-coated mMSCs and OP9s were an order of magnitude higher than the expected and actual yields of cells directly encapsulated without nanoparticle pre-coating (Fig. 2a). The yields were close to that achieved by fluorescence-activated cell sorting after encapsulation without pre-coating (FACS). Encapsulations at 4 °C and 25 °C produced similar degrees of efficiency and yield, and cells incubated at 4 °C did not uptake nanoparticles at detectable levels (Supplementary Fig. 1c,d), presumably due to a reduction in endocytosis[19]. Finally, the fraction of cells encapsulated in microgels (efficiency) was unaffected by the pre-coating process, and ranged from 0.93 to 0.95 for both cell types (Fig. 2b).

The integrity and homogeneity of the hydrogel layer surrounding cells, as well as the microgels' ability to support cell viability, were next analysed. Using alginates that had been conjugated with a fluorophore, the hydrogel layer that had formed around each encapsulated cell was visualized (Fig. 2c). This layer was found to

[1]Wyss Institute for Biologically Inspired Engineering at Harvard University, Cambridge, Massachusetts 02138, USA. [2]School of Engineering and Applied Sciences, Harvard University, Cambridge, Massachusetts 02138, USA. [3]Department of Pharmacology and Department of Bioengineering, University of Illinois College of Medicine, Chicago, Illinois 60612, USA. [4]Department of Physics, Harvard University, Cambridge, Massachusetts 02138, USA. [5]Biomaterials and Tissue Engineering Laboratory, School of Life Science and Biotechnology, Dalian University of Technology, Dalian 116024, China. [†]These authors contributed equally to this work. *e-mail: mooneyd@seas.harvard.edu
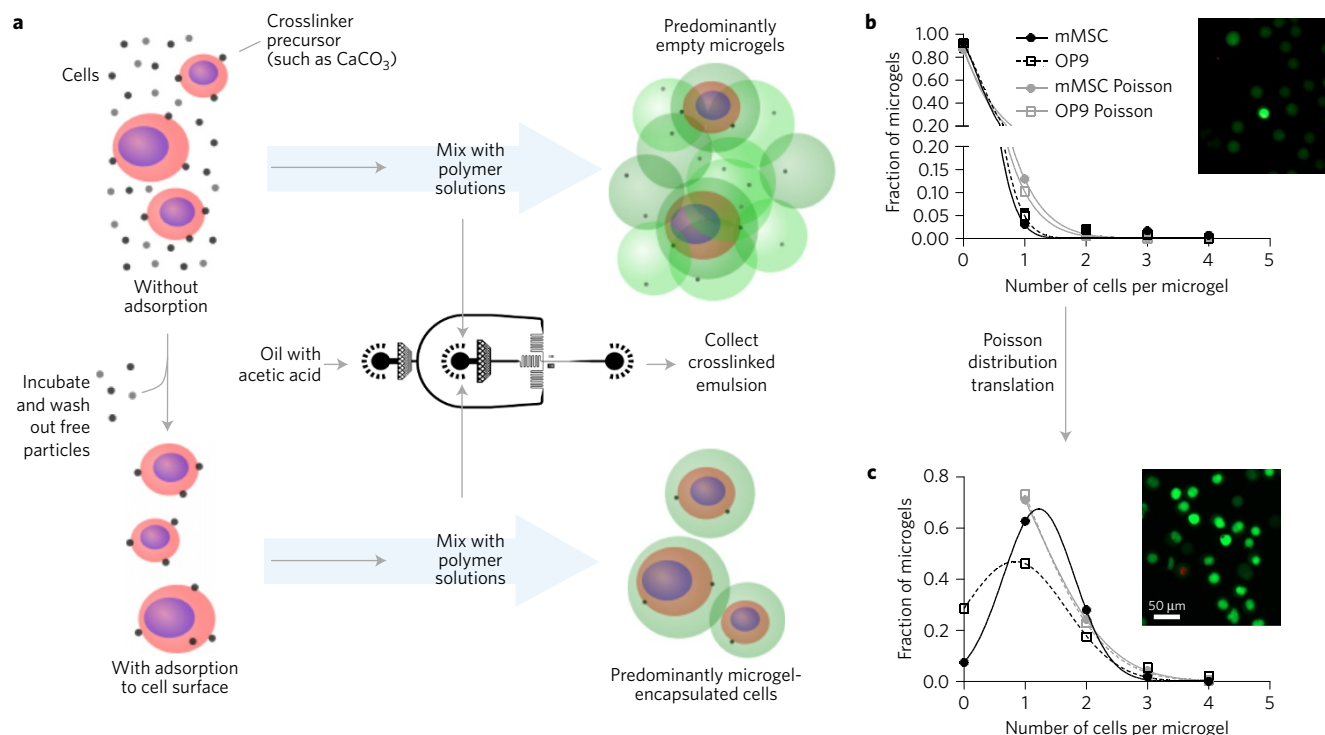
Figure 1 | Encapsulation of single cells in thin layers of alginate gel. a, Schematic showing steps in the encapsulation process. In pre-existing techniques (upper panel), cells are mixed with a crosslinker precursor, in this case calcium carbonate nanoparticles, and polymer solution, before being injected into a microfluidic device to form a water-in-oil emulsion. Diffusion from the oil phase into the aqueous phase of acetic acid catalyses soluble calcium release and polymer crosslinking. In this study, excess nanoparticles are removed from cell suspension before mixing with the polymer solution in a pre-coating step (lower panel), resulting in an emulsion consisting of predominantly microgel-encapsulating cells. **b**, Distribution of the fraction of microgels containing different numbers of cells, resulting from the microgel fabrication process using a cell, nanoparticle, and polymer suspension. Inset: mMSCs directly encapsulated in alginate without pre-coating with nanoparticles and stained for viability (green, alginate; bright green, live cells; red, dead cells). **c**, Distribution of fraction of microgels containing different numbers of cells, resulting from the microgel fabrication process using pre-coated cells. Inset: mMSCs pre-coated with nanoparticles and then encapsulated in alginate (green, alginate; bright green, live cells; red, dead cells). The theoretical Poisson distribution is also shown in **b** and **c**.

average 5.8 μm in thickness, as assessed by confocal microscopy (Fig. 2d). In this formulation, an average 16.1-μm-diameter mMSC represents 25% of the total encapsulate volume, similar to tissue densities, although this value shrinks to ~2% when cells are encapsulated singly in 60 μm microgels or bulk hydrogels at a typical density of 10 million cells ml^{-1}. Both the alginate content within the microgel (Fig. 2e), as assessed by image analysis of confocal slices, and the population of cell-encapsulating microgels (Fig. 2f), as assessed by flow cytometry, followed a unimodal distribution. The coefficient of variation (CV) of microgel size was 6.5%, falling within a quasi-monodisperse distribution[20]. Microgel size and dispersity were found to be unaffected by the pre-coating procedure (Fig. 2g). Nanoparticle concentration either adsorbed to cells or in suspension, as in empty microgels, did not affect microgel size or dispersity, except at very low concentrations of nanoparticles adsorbed to cells, which led to reduced microgel size (Fig. 2g and Supplementary Fig. 1e). This may be due to insufficient calcium ions released from the cell surface to crosslink the entirety of alginate in the droplet in this situation, leading to a slightly thinner hydrogel layer. Cells incubated with very low concentrations of nanoparticles and encapsulated without washing also resulted in a far lower efficiency of cell-containing microgels (16% efficiency at a nanoparticle concentration equivalent to 3.3% of that used in the rest of this study), presumably because many cell-containing droplets lacked enough calcium carbonate to crosslink the polymer. Acetic acid was mixed into the oil and surfactant phase prior to injection to immediately crosslink the alginate microgel upon emulsion formation so that cell viability can be maximized (Supplementary Fig. 1f).

Various acetic acid concentrations were tested for cytotoxicity, and only a concentration with minimal effect on cell viability was used for subsequent experiments (Supplementary Fig. 1g). The usage of calcium carbonate nanoparticles to crosslink alginate was also found not to significantly affect intracellular calcium levels of encapsulated cells (Supplementary Fig. 1h). mMSCs and OP9s were found to exhibit high viability both one and three days after encapsulation into arginine-glycine-aspartic acid (RGD)-modified alginates (Fig. 2h and Supplementary Fig. 1i)[21]. Addition of 20% of the aliphatic compound 1H,1H,2H,2H-perfluorooctanol (PFO) was sufficient for oil demulsification without decreasing cell viability (Supplementary Fig. 1j). To test if variations in microgel thickness would affect diffusion of soluble factors, diffusion of model dextran molecules was assessed by fluorescence recovery after photobleaching. No statistically significant differences in diffusion were found (Supplementary Fig. 1k–m). Moreover, as the inside-out crosslinking may potentially produce a gradient of polymer, alginate intensity in the radial direction was measured and the linear regressions calculated. Alginate content was found to be consistent across the thickness of the microgel layer (Supplementary Fig. 1n,o).

As alginate hydrogels are formed with reversible ionic crosslinks, cell-mediated gel remodelling[22] could potentially allow space for cell divisions within and mediate cell egress from microgels over time. To vary the mechanical resistance to remodelling, the polymer molecular weight was varied from the original average weight of 139 kDa, to both higher (232 kDa) and lower (48 kDa, 54 kDa) molecular weight (MW) polymers (Supplementary Fig. 2a–e). To
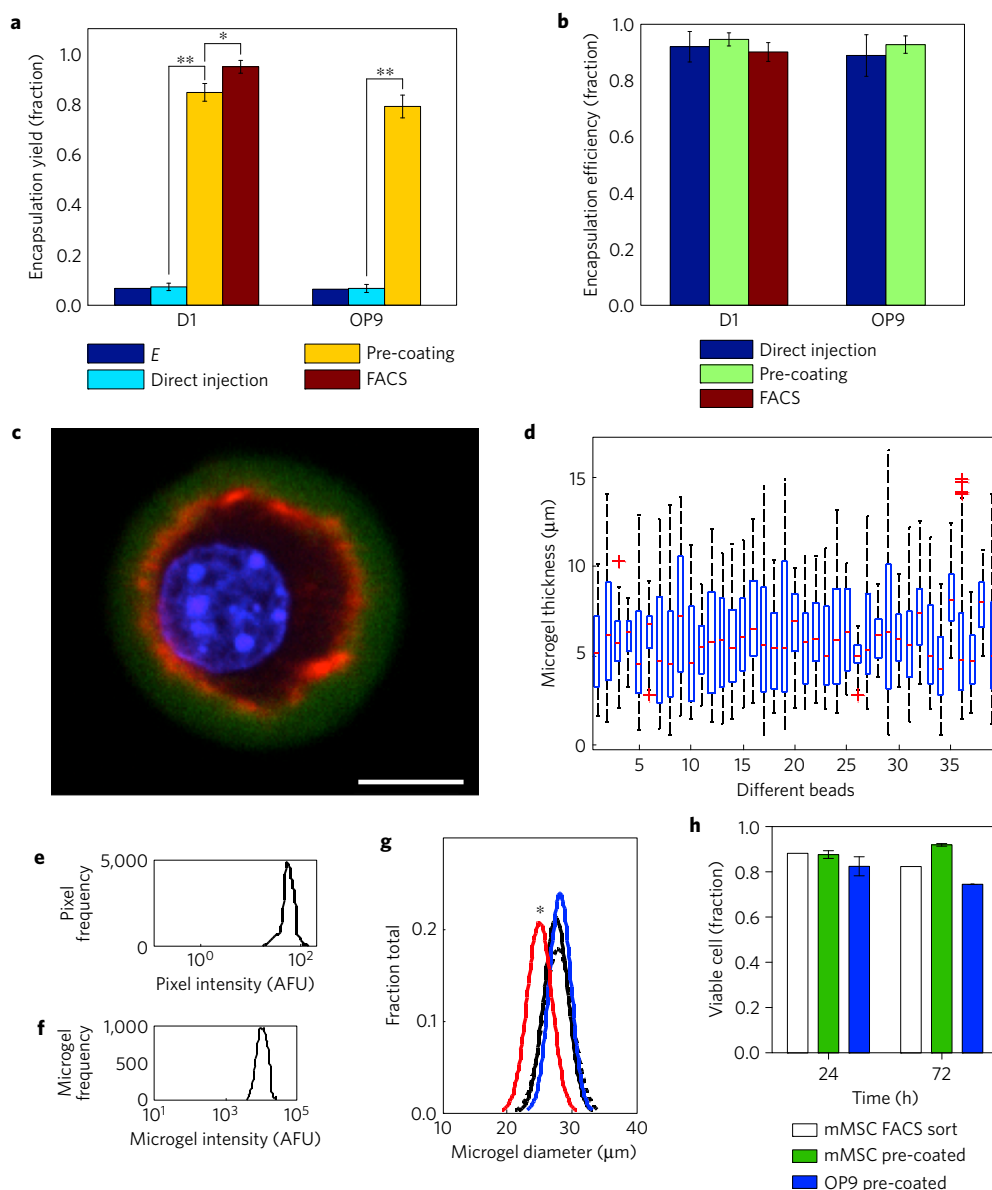
Figure 2 | Characterization of cell-encapsulating microgels. a, Fraction of alginate beads containing encapsulated mMSCs and OP9 cells (yield) by direct encapsulation, direct encapsulation followed by FACS, and pre-coating with $CaCO_3$ nanoparticles. E denotes theoretical yield from direct encapsulation. *, $p < 0.05$; **, $p < 0.01$; one-way analysis of variance (ANOVA) followed by Tukey's multiple comparison test. **b**, Fraction of mMSCs and OP9 cells encapsulated in microgels (efficiency) by direct encapsulation, direct encapsulation followed by FACS to generate a pure population, and pre-coating with $CaCO_3$ nanoparticles before encapsulation. **c**, Confocal slice of encapsulated mMSC (green, alginate; red, actin; blue, nucleus). Scale bar, 10 μm. **d**, Thickness of hydrogel layer, measured at multiple locations around cells, for 39 encapsulated mMSCs. The red crosses denote inner fence outliers, as assessed by Tukey's schematic boxplot. **e**, Histogram of alginate intensity per pixel taken from confocal images of 16 different cell-encapsulating alginate microgels, fabricated using the pre-coating method. The single peak indicates homogeneity within the microgel. **f**, Histogram of alginate intensity from 40,475 events consisting of the encapsulation output after pre-coating cells with nanoparticles. **g**, Size distribution of cell-encapsulating microgels. Solid red, black and blue lines show distributions of cell-encapsulating microgels exposed to 0.66, 3.3 and 17 g l^{-1} of $CaCO_3$ nanoparticles, respectively. Dotted black lines show distribution of microgels containing cells encapsulated without removal of unbound nanoparticles. *, $p < 0.05$, one-way analysis of variance (ANOVA) followed by Tukey's multiple comparison test. **h**, Viability of encapsulated cells one day and three days after encapsulation using pre-coating with nanoparticles (for mMSCs and OP9s), and with direct injection without pre-coating followed by a FACS sort (for mMSCs). Error bars where indicated refer to the standard error of the mean (s.e.m.) of three experimental runs, with ≥85 microgels or cells analysed per condition in each replicate run.

further confine cells, 232 kDa alginates were modified to enable covalent crosslinking via alginate modification with click reagents[23]. Specifically, ionic encapsulation in alginates modified with the click reagent tetrazine was followed by incubation in a solution of alginate conjugated with a complement reagent, norbornene. The covalent crosslinks formed between norbornene and tetrazine groups on the alginate would presumably inhibit matrix remodelling. The encapsulation efficiency and yield, and the viability of encapsulated

cells in these types of alginate, were assessed (Supplementary Fig. 2f,g). Although single cells were initially present in the microgels, significantly more cells per microgel were found after three days of culture in the lower-MW polymers, as compared to the 232 kDa polymer microgels (Fig. 3a and Supplementary Fig. 2h–l). However, microgel diameters at all three MW were found not to significantly change over the three days of culture, despite the increase in cell number in microgels formed from the
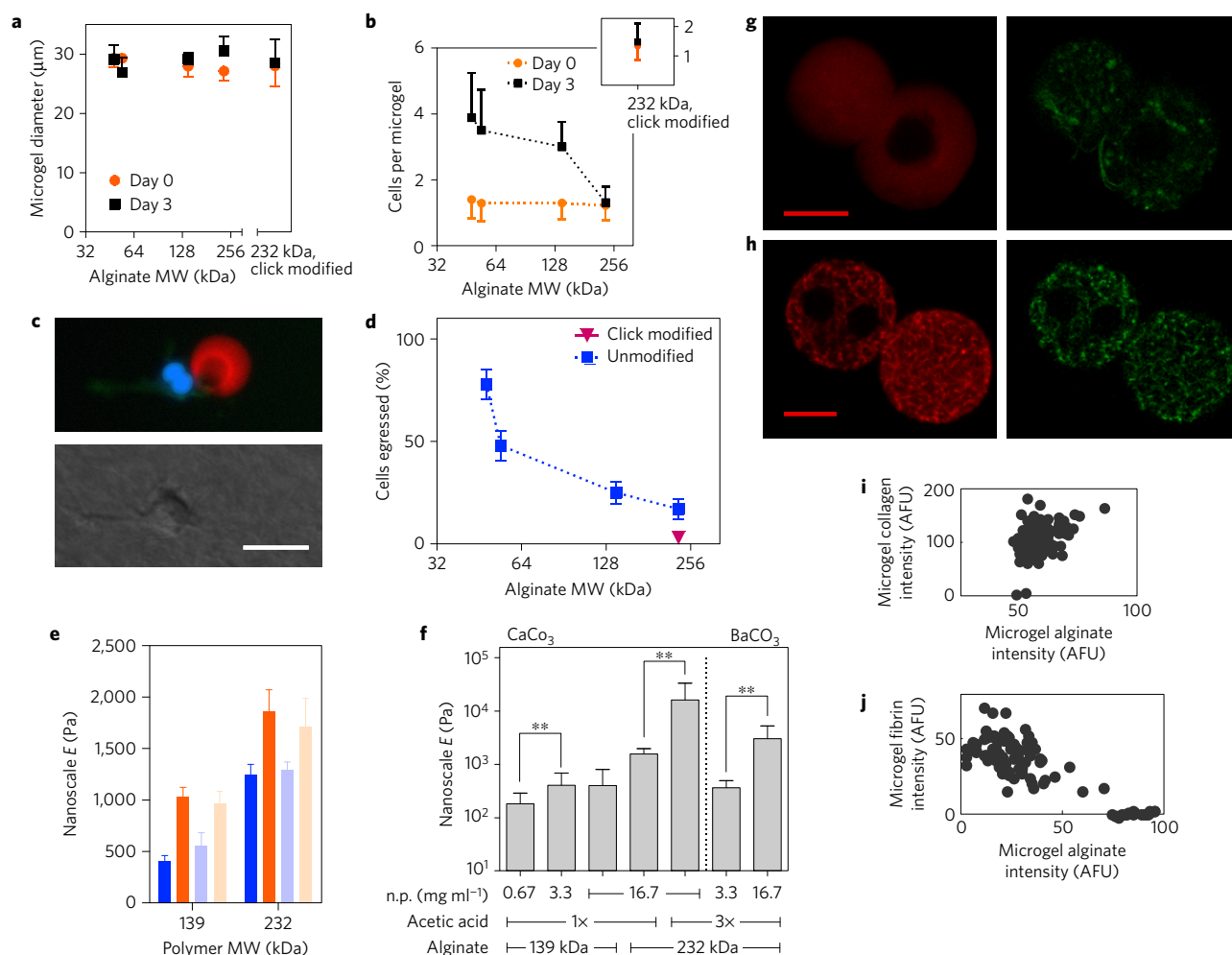
Figure 3 | Modulating polymer composition and mechanical properties of microgels to impact cell behaviour *in vitro*. a,b, The average microgel size (**a**, $n \geq 16$) as well as the average number of cells per microgel (**b**, $n \geq 18$) both initially and after three days of culture. The average number of cells per microgel after three days of culture differed significantly among microgels composed of alginates of different polymer weights (one-way ANOVA, $p < 0.01$). Microgel diameter, however, did not change significantly over the three-day culture. **c,** Fluorescent image (top) and bright-field image (bottom) of a cell leaving its microgel. Red, alginate; blue, nucleus; green, actin; scale bar, 50 μm. **d,** The fraction of cells that have egressed from microgels formed from alginates of different molecular weight and with click modification into surrounding collagen gel. Differences between conditions were statistically significant (chi-square test, df = 2, $p < 0.01$). $n \geq 47$, ± s.d. **e,** Elastic moduli of microgels as a function of polymer molecular weights, presence of cell within microgel, and post-encapsulation exposure to varying concentrations of additional calcium chloride after microgel formation (N-way ANOVA, $p < 0.01$). Blue and pale blue squares, 2 mM calcium chloride exposure; orange and pale orange squares, 15 mM calcium chloride exposure. Whited-out colours denote empty microgels. **f,** Elastic moduli of microgels as a function of different concentrations of nanoparticles incubated with cells during adsorption, exposure to different concentrations of acetic acid during microgel fabrication, and different molecular weights (**, $p < 0.01$, two-tailed *t*-test). For **e** and **f**, $n = 20$. **g,h,** Confocal images of alginate–collagen microgels (**g**; green, collagen; red, alginate) and alginate–fibrin (**h**; red, alginate; green, fibrin), scale bar, 20 μm. **i,** Scatter plot of mean fluorescence intensity of individual microgels, in terms of both collagen and alginate, for collagen–alginate microgels ($n = 168$). **j,** Scatter plot of mean fluorescence intensity of individual microgels, in terms of both fibrin and alginate, for fibrin–alginate microgels ($n = 103$). Error bars denote standard deviation (s.d.). *n* denotes number of microgels or cells analysed.

two-lower MW alginates and concomitant increase in cell cluster size (Fig. 3b). Microgels were also embedded within a collagen gel to mimic deposition within a tissue, and after one day of culture the fraction of cells that had exited microgels was determined (Fig. 3c). The fraction of egressed cells was significantly higher in 54 kDa and 48 kDa alginate microgels than in microgels formed from 139 kDa and 232 kDa alginate (Fig. 3d), and least in 232 kDa alginate gels with click modifications. These results demonstrate that alteration of polymer molecular weight and inclusion of secondary crosslinking could control cell proliferation and release, without external stimuli[24] or secondary encapsulations.

Three-dimensional adhesion substrate properties such as stiffness and composition have been shown to potently influence cell behaviour[13,25], and would be desirable to control in cell-encapsulating

microgels. To modify their stiffness, cell-encapsulating microgels were further crosslinked after formation. This significantly increased the elastic moduli, as assessed by atomic force microscopy (AFM, see Methods). The moduli of empty microgels crosslinked with the same concentrations of calcium carbonate were also assessed, and were not significantly different from those of cell-containing microgels, indicating consistent crosslinking through the microgel volume (Fig. 3e). A similar trend was observed with bulk hydrogels, although AFM measurements of hydrogel moduli were consistently lower than those done by bulk compressive testing (Supplementary Fig. 2m). Changing the density of calcium carbonate nanoparticles adsorbed to the cell surface also produced changes in the elastic modulus of the coating hydrogel, although this effect saturated at higher concentrations of
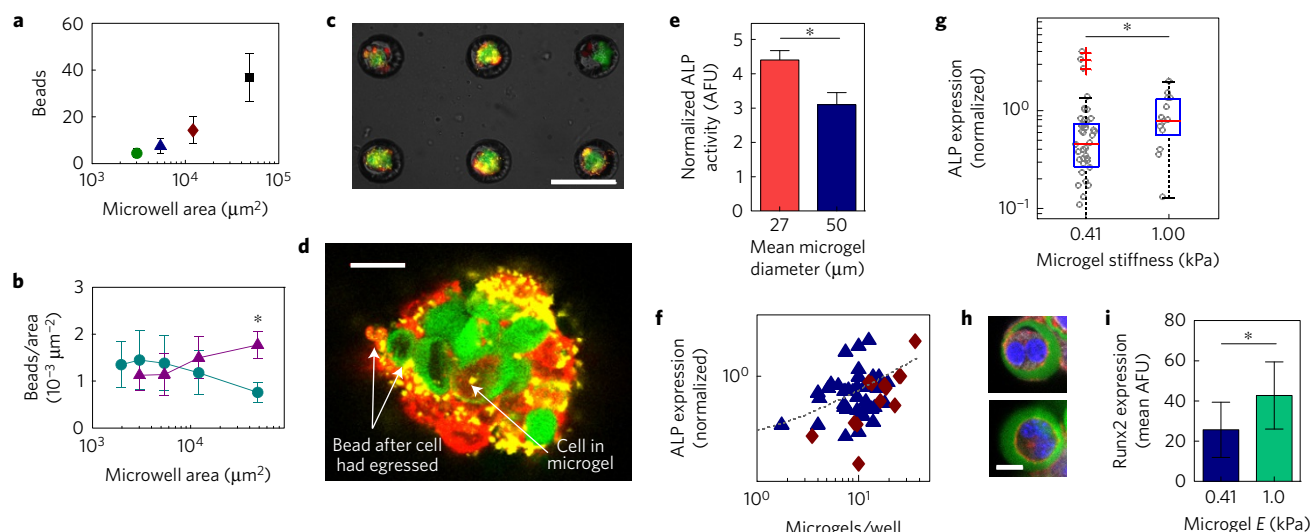
Figure 4 | Culture and differentiation of mMSC-encapsulating microgels in microwells. a, Number of microgels per 100-µm-deep microwell as a function of microwell area. **b**, Area density of microgels in PDMS microwells as a function of microwell area, in 100-µm-deep (circles) and 200-µm-deep (triangles) microwells. *, $p < 0.05$. For **a** and **b**, $n = 32$, 24, 20 and 4 for four different microwell diameters, in increasing size, ± s.d. **c**, Cells encapsulated in FITC-tagged alginate stained, after six days of culture, with actin (red) and an ALP marker (yellow); scale bar, 100 µm. **d**, Confocal imaging reveals some cells still inside microgels, and others that have egressed; scale bar, 20 µm. **e**, ALP production in cells encapsulated in microgels of different diameter. Two-tailed t-test, $p < 0.05$. $n \geq 18$ microgels, ± s.d. **f**, Log–log plot of alkaline phosphatase expression by encapsulated mMSCs normalized to microgel number after six days of culture as a function of the number of microgels per microwell, $r = 0.39$, $p < 0.01$. Black line shows least-square fit ($0.051x + 0.083$). $n = 59$ microwells. The symbols in **f** correspond to the different microwell sizes used in **a**. **g**, Box plot of ALP expression normalized to cell number in microgels with nanoscale stiffness 1.0 or 0.41 kPa, *, $p < 0.05$, Wilcoxon Rank Sum Test. $n = 13$ microwells. The red crosses denote inner fence outliers, as assessed by Tukey's schematic boxplot. **h**, Confocal images of encapsulated mMSC after three days of culture in a microgel of $E = 1.0$ (above) and $E = 0.41$ (below). Blue, nuclei; green, alginate; red, actin; white, runx2; scale bar, 10 µm. **i**, Intensity average of runx2 signal per microgel of different moduli. Two-tailed t-test, $p < 0.05$. $n = 11$ cells, ± s.d.

adsorbed nanoparticles. However, exposing microgels to increased acetic acid concentrations during fabrication in conjunction with increased nanoparticle concentrations produced substantially stiffer microgels. A similar trend was observed using barium carbonate nanoparticles. Finally, by combining higher nanoparticle concentrations, increased acetic acid concentration, and increased molecular weight, cell-encapsulating microgels of ~16 kPa were achieved (Fig. 3f and Supplementary Fig. 2n).

As inclusion of natural extracellular matrix (ECM) molecules may allow a greater control of cellular functions than synthetic peptides[25], the formation of collagen–alginate and fibrin–alginate hybrid microgels was explored. As fibrin crosslinking relies on the catalytic action of thrombin, a new microfluidic device was developed to allow one liquid stream containing the fibrin and alginate to be combined with a second containing thrombin alone immediately before droplet formation (Supplementary Fig. 3a); collagen–alginate microgels were formed in the same device as pure alginate microgels (Supplementary Fig. 3b). Confocal microscopy revealed collagen and fibrin fibrils within their respective microgels (Fig. 3g,h). The collagen and alginate, and fibrin and alginate components per microgel, respectively, appeared to follow unimodal distributions, with a CV of 8.6% for alginate and 24% for collagen (Fig. 3i,j). The alginate component was found to be evenly distributed in these formulations, and encapsulated cells underwent increased proliferation as compared to cells in microgels composed of alginate alone (Supplementary Fig. 3c–f). As the fibrin was observed to crosslink quickly, fibrin-only microgels were also fabricated (Supplementary Fig. 3e–g). Collagen–alginate, fibrin–alginate, and fibrin microgels were found to maintain cell viability over three days of culture, although to varying degrees (Supplementary Fig. 3h).

Singly encapsulated cells may provide a platform to assemble small-scale tissues, and study the impact of cell density on cell fate.

Microwells of polydimethylsiloxane (PDMS) were used to template and culture encapsulated cells, and the number of cells in each microwell ranged from 2.6 to 37 cells per well as the microwell size was varied, with uniform microgel density within each microwell size (Fig. 4a,b). Encapsulated mMSCs were cultured for six days and analysed for early osteogenesis, as indicated by alkaline phosphatase (ALP) expression (Fig. 4c, see Methods). Confocal imaging revealed a combination of cells that had remained inside microgels, and egressed cells that had colonized the outside surfaces of microgels (Fig. 4d). Increased differentiation per cell was observed in singly encapsulated mMSCs, compared to larger microgels encapsulating multiple mMSCs that were seeded into microwells of the same diameter. This is presumably a result of the higher ratio of cell to hydrogel matrix in singly encapsulated cells, which allows for an increased cell density closer to that found in tissue (Fig. 4e and Supplementary Fig. 4a,b). ALP expression, normalized to cell number, was found to significantly correlate with the initial number of cell-encapsulated microgels per well (Fig. 4f), indicating that cell assemblage size impacts osteogenic differentiation. Moreover, increased osteogenesis, as assessed by the expression of ALP and the osteogenic transcription factor runx2, was observed in cells encapsulated in stiffer microgels compared to softer microgels (Fig. 4g–i), thereby recapitulating past results observed with large populations of MSCs (~10^6 cells) encapsulated in bulk hydrogels[13].

Our method may enable large-scale production of uniformly coated single cells for therapies where cells are administered to patients, and improve upon existing methods utilizing polymeric encapsulation to extend cell residence[26–29]. Donor cells encapsulated in microgels and lodged in lung capillaries after intravenous (i.v.) injection[30] are expected to be protected from shear force and immune clearance so that they can secrete factors into circulation in a more sustained manner (Fig. 5a). To first determine if microgels could retain structural integrity in circulation, they
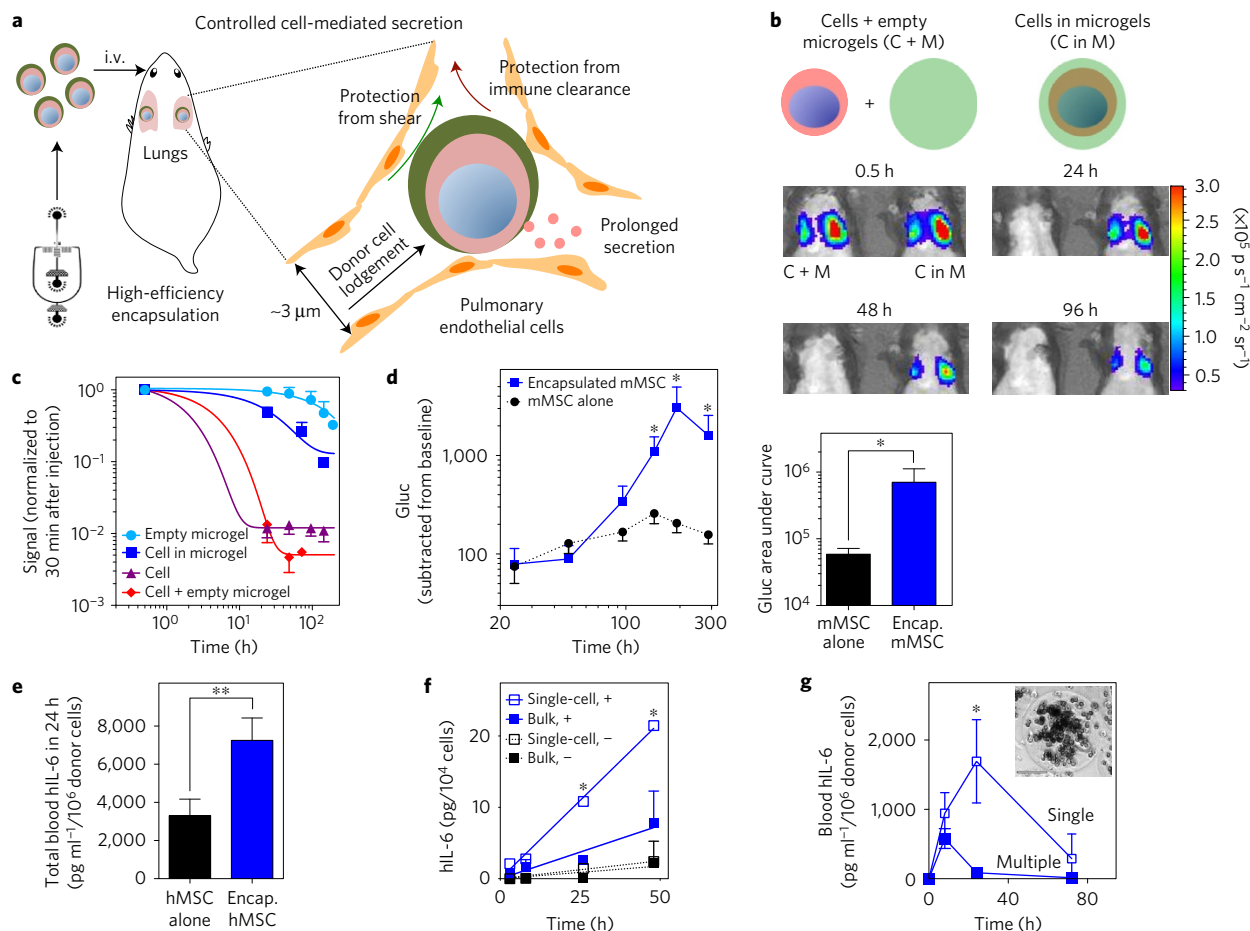
Figure 5 | Microgel encapsulation prolongs the *in vivo* residence time of donor cells and systemic levels of secreted soluble factors after i.v. injection.
a, Schematics demonstrating a therapeutic modality using singly encapsulated cells injected intravenously. **b**, Representative bioluminescence images showing the biodistribution of mMSCs overexpressing Firefly luciferase with or without microgel encapsulation after i.v. injection. **c**, The clearance kinetics of singly encapsulated mMSCs after i.v. injection compared to cells alone, cells mixed with microgels, and empty microgels. For each group, all the values were normalized by the value at 30 min. The signals from lungs were measured. The fluorescence signals were measured for empty microgels, whereas the luminescence signals were measured for microgels that contained cells. The data were fitted to $Y = (1.00 - Plateau) \times exp(-k \times t) + Plateau$. For each group half-life ($t_{1/2} = ln(2)/k$) is: Empty microgel = 142.6 hr; Cell in microgel = 30.74 hr; Cell = 2.59 hr; Cell + empty microgel = 2.85 hr. $n \geq 5$ recipients. **d**, Left: blood plasma levels of Gaussia luciferase after i.v. injection of engineered mMSCs with or without microgel encapsulation. Right: total Gaussia luciferase produced over 300 h as indicated by area under curve. Student's *t*-test, $^*P < 0.05$, $n \geq 6$ recipients. **e**, Blood plasma levels of human IL-6 after i.v. injection of hMSCs into the NOD/SCID/IL2γ$^{-/-}$ (NSG) mice. Total human IL-6 level in blood (pg ml^{-1}) over 24 h after injection of 0.2–0.3 million hMSCs per mouse. Student's *t*-test, $^{**}P < 0.005$. $n \geq 4$ recipients. **f**, *In vitro* human IL-6 secretion kinetics from hMSCs encapsulated in either bulk gels or single microgels. −: unstimulated, +: IFNγ (100 ng ml^{-1}). $n = 2$, ± s.d. **g**, *In vivo* human IL-6 secretion kinetics from single or multiple hMSCs in microgels. Inset: representative image showing a microgel that encapsulates multiple hMSCs with ∼250 μm diameter. Cell-encapsulating microgels were stimulated *ex vivo* with IFNα (100 ng ml^{-1}) overnight, washed out, and i.v. injected into NSG mice. $n = 4$ mice for single, $n = 9$ for multiple, from two independent experiments, ± s.e.m. For both **f** and **g**, two-way ANOVA $P < 0.05$, followed by Bonferroni's multiple comparisons test, $^*P < 0.05$, single versus multiple or bulk, stimulated.

were subjected to *in vitro* shear forces ten times higher than arterial pressure (∼2 Pa) using a cone-plate rheometer. Even soft ($E = \sim 300$ Pa) microgels were found to withstand this level of shear (Supplementary Fig. 5a).

Consistent with previous observations[30], Balb/c mMSCs were localized in lungs of C57/BL6 mice shortly after i.v. injection. Strikingly, the half-life of donor cell clearance was increased by a factor of approximately ten when cells were encapsulated in soft 120 kDa alginate microgels (∼300 Pa), but not when cells were mixed with empty microgels (Fig. 5b,c, see Methods). This finding indicates that encapsulation of allogeneic donor cells dramatically improves their maintenance *in vivo* after i.v. injection. Microgel-encapsulated cells can also be delivered via the intraperitoneal route (Supplementary Fig. 5b). A similar high yield and encapsulation efficiency were obtained with human MSCs (hMSCs) (Supplementary Fig. 5c).

Microgel encapsulation again resulted in a dramatic increase in the residence time of the hMSCs after i.v. injection into the NOD/SCID/IL2γ$^{-/-}$ (NSG) mice (Supplementary Fig. 5d). Interestingly, hMSCs were cleared more slowly, by a factor of approximately two, than the injection of mMSCs into immunocompetent mice. Hydrogel encapsulation even enhanced the bioluminescence signal from the initial input after a day of injection in this model.

Although microgel-encapsulated cells demonstrated a dramatic increase in half-life *in vivo*, they were eventually cleared over time. Cell-free alginate microgels showed a five times longer residence time following i.v. injection than encapsulated cells (Fig. 5c), suggesting that clearance of encapsulated cells was not due to that of alginate degradation. More than 90% of the encapsulated cells remained viable *in vitro* within 72 h (Fig. 2h), suggesting that mMSC clearance *in vivo* was also probably not a result of cell death in

encapsulates. In contrast, the half-time of *in vitro* cell egress from 139 kDa alginate microgels is estimated to be ∼60 h (Fig. 3d), suggesting that the kinetics of cell egress from microgels may determine that of cell clearance *in vivo*. To investigate whether host immunity regulates clearance of donor cells, mMSCs were i.v. infused into syngeneic mice. mMSCs cells were cleared from lungs in syngeneic recipients to a similar extent as found earlier in allogeneic recipients, and encapsulation led to a similar increase in the clearance half-life (Supplementary Fig. 5e). This finding suggests adaptive immunity is probably not a contributing factor to cell clearance.

Studies were next performed to test whether prolonged cell delivery was accompanied by the sustained systemic presence of soluble factors from donor cells. mMSCs were genetically modified to express Gaussia luciferase (Gluc, ∼20 kD), which is constitutively secreted[31]. Intravenous injection of encapsulated cells led to a progressive increase in blood Gluc levels, with a peak at week 2 (Fig. 5d). In contrast, injection of unencapsulated cells led to much lower blood levels of Gluc; the total amount of Gluc in blood over two weeks was increased by a factor of approximately ten with encapsulation. To evaluate whether this approach also results in sustained systemic secretion of native soluble factors from donor cells, singly encapsulated hMSCs were i.v. injected into NSG mice. The encapsulation procedure did not compromise IL-6 secretion by hMSCs, either constitutively or under stimulation by IFNγ (Supplementary Fig. 5f). Injection of encapsulated cells increased the total concentration of human IL-6 in blood plasma at 24 h by a factor of approximately two, as compared to unencapsulated cells (Fig. 5e). Analogous to controlled release of small drug molecules by polymeric nanoparticles, high-yield microgel encapsulation of single cells is thus anticipated to deliver secreted soluble factors in a more sustained manner.

Finally, we evaluated whether single-cell encapsulation offers potential advantages over gels containing multiple cells in terms of cytokine secretions. No difference was observed in IL-6 secretion kinetics *in vitro* under a basal condition between single- and bulk-cell encapsulation. However, IFNγ exposure increases IL-6 secretions from singly encapsulated hMSCs to a greater extent than those from bulk gels (Fig. 5f). Although MSCs within a thinner gel coating could have a more immediate access to exogenous factors than those in bulk gels, the diffusion half-life of <50 kDa soluble proteins through alginate hydrogels is just a few hours[13]. If the only difference between single-cell and bulk-cell encapsulation is the diffusion rate of exogenous factors, it is expected that IL-6 secretion from bulk gels will reach the same level as that from single-cell encapsulation over time. However, both single- and bulk-encapsulated hMSCs show linear IL-6 secretion kinetics (Fig. 5f). This raises a possibility that single-cell encapsulation could alter biological pathways to enhance sensitivity towards exogenous stimuli. Consistent with the *in vitro* results, singly encapsulated, *ex vivo* IFNγ-primed hMSCs show enhanced IL-6 secretion into blood plasma after i.v. injection, compared to microgels containing multiple cells (Fig. 5g). The relatively large size (∼250 μm) of these microgels did not cause any adverse effect on the overall health of the recipients after i.v. injection. Overall, the results suggest that decreasing material-to-cell volume ratio does not simply change steady-state cytokine diffusion from cells in gels, but rather enhances the ability of encapsulated cells to respond to exogenous stimuli.

The results of this study provide several advancements to the field of microencapsulation, including single-cell encapsulation within a thin hydrogel layer, a one-step method for dramatically increasing the fraction of microgels containing cells, control over micromechanical properties of the hydrogel matrix, and fabrication of cell-encapsulating hybrid microgels. The approach presented here may abet regenerative medicine applications by enabling control of tissue assembly and cell delivery at the single-cell level, and combining the ease of injections with control over cellular functions using hydrogel encapsulation.

Methods

Methods and any associated references are available in the online version of the paper.

References

1. Selimovic, S., Oh, J., Bae, H., Dokmeci, M. & Khademhosseini, A. Microscale strategies for generating cell-encapsulating hydrogels. *Polymers* **4,** 1554 (2012).
2. Martinez, C. J. *et al*. A microfluidic approach to encapsulate living cells in uniform alginate hydrogel microparticles. *Macromol. Biosci.* **12,** 946–951 (2012).
3. Tan, W. H. & Takeuchi, S. Monodisperse alginate hydrogel microbeads for cell encapsulation. *Adv. Mater.* **19,** 2696–2701 (2007).
4. Chung, B. G., Lee, K., Khademhosseini, A. & Lee, S. Microfluidic fabrication of microengineered hydrogels and their application in tissue engineering. *Lab Chip* **12,** 45–59 (2012).
5. Velasco, D., Tumarkin, E. & Kumacheva, E. Microfluidic encapsulation of cells in polymer microgels. *Small* **8,** 1633–1642 (2012).
6. Wu, L., Chen, P., Dong, Y., Feng, X. & Liu, B. F. Encapsulation of single cells on a microfluidic device integrating droplet generation with fluorescence-activated droplet sorting. *Biomed. Microdevices* **15,** 553–560 (2013).
7. Edd, J. F. *et al*. Controlled encapsulation of single-cells into monodisperse picolitre drops. *Lab Chip* **8,** 1262–1264 (2008).
8. Kemna, E. W. M. *et al*. High-yield cell ordering and deterministic cell-in-droplet encapsulation using Dean flow in a curved microchannel. *Lab Chip* **12,** 2881–2997 (2012).
9. Veerabadran, N. G., Goli, P. L., Stewart-Clark, S. S., Lvov, Y. M. & Mills, D. K. Nanoencapsulation of stem cells within polyelectrolyte multilayer shells. *Macromol. Biosci.* **7,** 877–882 (2007).
10. Wilson, J. T. *et al*. Cell surface engineering with polyelectrolyte multilayer thin films. *J. Am. Chem. Soc.* **133,** 7054–7064 (2011).
11. Tatsumi, K. *et al*. The non-invasive cell surface modification of hepatocytes with PEG-lipid derivatives. *Biomaterials* **33,** 821–828 (2012).
12. Teramura, Y., Oommen, O. P., Olerud, J., Hilborn, J. & Nilsson, B. Microencapsulation of cells, including islets, within stable ultra-thin membranes of maleimide-conjugated PEG-lipid with multifunctional crosslinkers. *Biomaterials* **34,** 2683–2693 (2013).
13. Huebsch, N. *et al*. Harnessing traction-mediated manipulation of the cell/matrix interface to control stem-cell fate. *Nat. Mater.* **9,** 518–526 (2010).
14. Lee, Y. L. & Mooney, D. J. Alginate: properties and biomedical applications. *Prog. Polym. Sci.* **37,** 106–126 (2012).
15. Köster, S. *et al*. Drop-based microfluidic devices for encapsulation of single cells. *Lab Chip* **8,** 1110–1115 (2008).
16. Holtze, C. *et al*. Biocompatible surfactants for water-in-fluorocarbon emulsions. *Lab Chip* **8,** 1632–1639 (2008).
17. Nakano, T., Kodama, H. & Honjo, T. Generation of lymphohematopoietic cells from embryonic stem cells in culture. *Science* **265,** 1098–1101 (1994).
18. Choi, K. *et al*. Hematopoietic and endothelial differentiation of human induced pluripotent stem cells. *Stem Cells* **27,** 559–567 (2009).
19. Fernando, L. P. *et al*. Mechanism of cellular uptake of highly fluorescent conjugated polymer nanoparticles. *Biomacromolecules* **11,** 2675–2682 (2010).
20. De la Vega, J. C., Elischer, P., Schneider, T. & Häfeli, U. O. Uniform polymer microspheres: monodispersity criteria, methods of formation and applications. *Nanomedicine* **8,** 265–285 (2013).
21. Rowley, J. A., Madlambayan, G. & Mooney, D. J. Alginate hydrogels as synthetic extracellular matrix materials. *Biomaterials* **20,** 45–53 (1999).
22. Chaudhuri, O. *et al*. Substrate stress relaxation regulates cell spreading. *Nat. Commun.* **6,** 6365 (2015).
23. Desai, R. M. *et al*. Versatile click alginate hydrogels crosslinked via tetrazine-norbornene chemistry. *Biomaterials* **20,** 30–37 (2015).
24. Steinhilber, D. *et al*. A microgel construction kit for bioorthogonal encapsulation and pH-controlled release of living cells. *Angew. Chem. Int. Ed.* **52,** 13538–13543 (2013).
25. Chaudhuri, O. *et al*. Extracellular matrix stiffness and composition jointly regulate the induction of malignant phenotypes in mammary epithelium. *Nat. Mater.* **13,** 970–978 (2014).
26. Karoubi, G., Ormiston, M. I., Stewart, D. J. & Courtman, D. W. Single-cell hydrogel encapsulation for enhanced survival of human marrow stromal cells. *Biomaterials* **30,** 5445–5455 (2009).
27. Orive, G. *et al*. Cell encapsulation: promise and progress. *Nat. Med.* **9,** 104–107 (2003).
28. Ma, M. *et al*. Core-shell hydrogel microcapsules for improved islets encapsulation. *Adv. Healthc. Mater.* **2,** 667–672 (2013).

29. Pareta, R. A., McQuilling, J. P., Farney, A. C. & Opara, E. C. in *Regenerative Medicine Applications in Organ Transplantation* 1st edn (eds Orlando, G., Lerut, J., Soker, S. & Stratta, R. J.) 627–635 (Academic, 2014).
30. Fischer, U. M. *et al*. Pulmonary passage is a major obstacle for intravenous stem cell delivery: the pulmonary first-pass effect. *Stem Cells Dev.* **18,** 683–691 (2009).
31. Wurdinger, T. A secreted luciferase for *ex vivo* monitoring of *in vivo* processes. *Nat. Methods* **5,** 171–173 (2008).

Author contributions

A.S.M., J.-W.S. and D.J.M. conceived and designed the experiments. S.U., H.W. and D.A.W. contributed to microfluidic design and fabrication. A.S.M. and J.-W.S. performed the experiments. A.S.M., J.-W.S. and D.J.M. analysed the data. A.S.M., J.-W.S. and D.J.M. wrote the manuscript. All authors discussed the results and commented on the manuscript. A.S.M. and J.-W.S. contributed equally to this work. The principal investigator is D.J.M.

Additional information

Supplementary information is available in the online version of the paper. Reprints and permissions information is available online at www.nature.com/reprints. Correspondence and requests for materials should be addressed to D.J.M.

Competing financial interests

The authors declare no competing financial interests.

Methods

Microfluidic device and microwell fabrication. Soft lithography was used to fabricate microfluidic devices, as described previously[9], and microwells. Negative photoresist SU-8 3025 (MicroChem) was deposited onto clean silica wafers to a thickness of 25 or 50 μm for devices, and 100 or 200 μm for microwells, and patterned by ultraviolet light exposure through a transparency photomask (CAD/Art Services, Bandon, Oregon). After the photoresist was developed, polydimethylsiloxane (PDMS) (Dow Corning) was mixed with crosslinker (ratio 10:1), degassed, poured, and cured for at least 1 h at 65 °C. For microfluidic devices, the PDMS replicas were peeled off the wafer and bonded to glass slides by oxygen-plasma activation of both surfaces. Microfluidic channels were then treated with Aquapel (PPG Industries). Polyethylene tubing with inner diameter 0.38 mm and outer diameter 1.09 mm, and 27G × 1/2 needles were used to connect channels to plastic syringes (all from Becton Dickinson).

To concentrate encapsulated cells during seeding into microwells, 3D-printed polyurethane fences were glued onto the borders of microwell field replicates using PDMS. Microwell fields consisted of 100 μm- or 200 μm-deep wells with diameters of 50, 83, 124, or 221 μm, arranged such that the total microwell surface area was constant per 750 μm × 750 μm field. Microwells were incubated in 70% ethanol for 2 h, washed with deionized H$_2$O, and treated with 3% Pluronic F68 overnight, followed by two washes of Dulbecco's phosphate buffered solution before use. Microgel-encapsulated cells were then seeded and allowed to settle by gravitational sedimentation for 1 h.

Alginate preparation. Sodium alginate with high (232 kDa) and medium (139 kDa) molecular weight and high guluronic acid content was purchased from FMC Biopolymer (Princeton, New Jersey). To produce the low-MW alginate, the high-MW alginate was gamma-irradiated with a cobalt-60 source at a gamma-dose of 3 Mrad. Alginates were covalently coupled with the integrin-binding peptide (Gly)4-Arg-Gly-Asp-Ala-Ser-Ser-Lys-Tyr (Peptides International) and either Fluoresceinamine, isomer I (Sigma-Aldrich) or Lissamine Rhodamine B Ethylenediamine (Setareh Biotech). 1-bicyclo[2.2.1]hept-5-en-2-ylmethanamine (norbornene; Matrix Scientific) or 3-(p-benzylamino)-1,2,4,5-tetrazine (Sigma-Aldrich) were prepared and conjugated to 232-kDa alginate as described previously[23].

Cell culture. Clonally derived mouse MSCs (D1s) purchased from American Type Cell Culture (ATCC) were expanded subconfluently in high-glucose, 10% fetal bovine serum-supplemented Dulbecco's Modified Eagle media (complete DMEM). OP9s were purchased from ATCC and expanded subconfluently in Alpha Minimum Essential Medium supplemented with 20% fetal bovine serum. Viability was assessed by cells with calcein-AM and ethidium homodimer-1 (Invitrogen, Eugene, Oregon) or Trypan Blue exclusion (Beckman Coulter). Human bone marrow aspirates were purchased from Lonza. hMSCs were then isolated using a standard plastic adherence protocol[14]. Briefly, mononuclear cells were isolated from bone marrow aspirates using gradient centrifugation with the Optiprep (StemCell Technologies). The cells were then cultured on plastic for 24 h. The non-adherent cell fraction was washed out four times with PBS. The adherent cells were then cultured in low-glucose DMEM + 10% FBS + 1% penicillin/streptomycin for approximately two weeks (Passage 0). Upon ~80% confluence, cells were passaged for expansion. A passage number up to 6 was used for the experiments. Human umbilical vein endothelial cells were purchased from Lonza and cultured in EGM-2 medium (Lonza). K-562 chronic myelogenous leukaemia cells were obtained from ATCC and cultured in Iscove's Modified Dulbecco's Medium, supplemented with 10% fetal bovine serum. Cell lines were assessed for mycoplasma contamination visually after staining with DAPI.

Encapsulation. Calcium carbonate nanoparticles (CalEssence(R) 70 PCC) or barium carbonate nanoparticles (US Research Nanomaterials) were suspended in HEPES-buffered complete DMEM (Sigma-Aldrich, St. Louis, Missouri) or HEPES-buffered physiological saline, dispersed by sonication with a Vibra Cell Sonicator at 70% amplitude, and purified by centrifugation or filtration. Cells were incubated in nanoparticle suspension for between 10 and 40 min with gentle agitation. To vary coverage of nanoparticles on cells, different concentrations of nanoparticles were incubated with cells. To measure calcium content of nanoparticles adsorbed to cells, nanoparticle-adsorbed cells were washed with calcium-free medium and then exposed to 3.7% hydrochloric acid (Sigma-Aldrich) or saline supplemented with 0.2 normal acetic acid. To measure the amount of uptaken calcium nanoparticles, cells were lysed using a Vibra Cell Sonicator at 40% amplitude for a total of 1.5 min into 0.2 normal acetic acid. The calcium concentration was then measured using a kit (Abcam). Excess nanoparticles were removed using centrifugation or filtration, and the coated cells were combined with polymer precursor solutions for injection. In direct injection experiments, cells at the same concentration as in pre-coated experiments were directly mixed with calcium carbonate nanoparticles before combining with alginate. The continuous phase was prepared by mixing 1% fluorosurfactant[8] and sterile-filtered acetic acid (EMD Chemicals) in a fluorinated oil (3M Novec Engineering Fluid HFE-7500). The continuous and aqueous phases were injected into the microfluidic device at flow rates of 3.2 μl min^{-1} and 1 μl min^{-1}, respectively. Devices with varying cross-sectional aperture dimensions at the cross-junction were used to achieve microgels of different dimensions. For most experiments, cells in microgels under 100 μm were incubated with 3.3 g l^{-1} nanoparticles and injected with 0.030% or 0.090% acetic acid, whereas cells in microgels over 100 μm were incubated with 6.6 g l^{-1} nanoparticles and injected with 0.060% acetic acid. Emulsions were broken after a 30 min incubation by the addition of 20% 1H,1H,2H,2H-perfluorooctanol (Alfa Aesar). Cells in bulk gel discs were encapsulated using a previously described method[14]. Briefly, alginate and a calcium sulfate slurry containing suspended cells were loaded into separate 3 ml syringes. The syringes were connected with a female–female Luer lock coupler (ValuePlastics), and the two solutions were rapidly mixed together with eight pumps of the syringe handles. The alginate was deposited on a glass plate and allowed to crosslink for 45 min.

To fabricate hybrid collagen–alginate microgels, a cell and polymer precursor suspension containing 3 mg ml^{-1} calcium carbonate nanoparticles, 0.93% 139 kDa alginate, and 0.66 mg ml^{-1} rat tail collagen I (Corning, Bedford, MA) was injected at 4 °C into a microfluidic device of the same design as that used for alginate microgels and operated with the same parameters. The resulting emulsion was incubated at 37 °C for 30 min. To fabricate hybrid fibrin–alginate microgels, two solutions were prepared: one combining fibrinogen (20.3 mg ml^{-1}) and aprotinin (45 μg ml^{-1}); and one combining calcium carbonate nanoparticles (6.7 mg ml^{-1}), 2.1% alginate, and thrombin (22 U ml^{-1}). Cells were suspended in the solution containing fibrinogen. The two aqueous phases and the continuous phase were injected into separate inlets of the microfluidic device at flow rates of 0.5 μl min^{-1} and 3.2 μl min^{-1}, respectively.

Analysis of cell egress. Alginate microgels encapsulating cells were themselves encapsulated in a bulk collagen hydrogel. Following manufacturer's instructions, rat tail collagen I (Santa Cruz Biotechnology) was first mixed with Dulbecco's phosphate buffered saline and sodium hydroxide to achieve a neutral pH, and then mixed with a suspension containing cells encapsulated in alginate microgels to obtain a final collagen concentration of 1.85 mg ml^{-1}. The suspension was added to wells in a 48-well plate and allowed to crosslink at 37 C for 30 min. Collagen gels were fixed after one or three days of culture. Cells were stained with rhodamine- or fluorescein-conjugated phalloidin (Biotium) and DAPI (Enzo Life Sciences, Plymouth Meeting, PA), and imaged with a Nikon E800 upright microscope. Only microgels that showed a morphology consistent with having previously contained cells (that is, hollowed out morphology) were considered to have led to cell egress.

Mechanical testing. Prior to atomic force microscopy measurement, microgels containing encapsulated cells in fluorescently labelled alginate were adhered to a polylysine-coated glass slide. Glass microscope slides (VWR International) were cleaned in a solution of 10% sodium hydroxide and 60% ethanol, rinsed with deionized water, and incubated with poly-L-lysine (Handary SA). To increase elastic moduli of hydrogels, cell-encapsulated microgels were exposed to 2 mM or 15 mM calcium chloride solutions (Sigma-Aldrich) for 15 min. Alternatively, cells were incubated with different concentrations of CaCO$_3$ for 45 min prior to the encapsulation procedure. Prior to measurement, cells were washed into a protein-free buffer (25 mM HEPES, 130 mM NaCl, 2 mM CaCl$_2$). An MFP-3D system (Asylum Research) was used to perform AFM measurements of the Young's modulus of hydrogels, using silicon nitride cantilevers (MLCT, Bruker AFM Probes). The stiffness was calibrated by determining a spring constant of the cantilever from the thermal fluctuations at room temperature, ranging from 20 ~ 50 mN m^{-1}. The cantilever was moved towards the stage at a rate of 1 μm s^{-1} for indentations, and indentations were made to the microgel surface. For bulk hydrogels, a disc of 5 mm × 2 mm was placed onto a PDMS mould on a glass slide. Force–indentation curves were fitted using the Hertzian model with a pyramid indenter. Bulk alginate gels were fabricated at 1% or 2% polymer concentration, with 20 mM or 50 mM final calcium content. The elastic modulus of bulk alginate hydrogels was measured by casting 10-mm-diameter and 2-mm-thick cylindrical discs and compressing without confinement using an Instron 3342 mechanical apparatus at 1 mm min^{-1}. To measure diffusion through alginate microgels, cell-encapsulating microgels were fixed and exposed to a solution containing fluorescein isothiocyanate-conjugated dextran molecules of varying molecular weight (Sigma-Aldrich, St. Louis, Missouri). A 1.7-μm-diameter area was bleached in different regions of the microgel shell, and the recovery was tracked using confocal microscopy (Upright Zeiss LSM 710). Recovery half-time was determined by fitting the normalized fluorescence recovery with a single exponential in MATLAB.

Osteogenic differentiation. To induce osteogenesis, mMSCs encapsulated in microgels were cultured with complete DMEM supplemented with 10 mM β-glycerophosphate and 250 μM L-ascorbic acid, cycling every two days. mMSCs were fixed after three days of culture and stained, permeabilized with

Triton X-100, blocked with 10% goat serum, and incubated with an AlexaFluor 647-conjugated Runx2 antibody overnight (Novus Biologicals). Imaging was performed with confocal microscopy (Upright Zeiss LSM 710). To assess ALP activity, mMSCs were fixed six days after osteogenic induction and stained with elf-97, following the manufacturer's instructions. Staining was stopped through washing with an excess of PBS after 90 s. Fixed cells were further stained with rhodamine-conjugated phalloidin (Biotium). Fluorescence images for immunohistochemistry, elf-97 staining, and alginate were acquired using an Olympus IX81 inverted microscope (BD Biosciences) and a Coolsnap HQ2 camera (Prior Scientific). The area-average fluorescence of cells stained with elf-97 and of alginate was quantified with ImageJ.

Expression of exogenous genes in cells. To introduce mCherry and Firefly luciferase in MSCs, lentiviral particles containing the vector with mCherry-IRES-Firefly luciferase driven by the CMV promoter were purchased from the Vector Core at Massachusetts General Hospital. Cells were incubated with viral particles for two days. Cells expressing mCherry were then sorted via flow-activated cell sorting (FACS). In some cases, cyan fluorescence protein (CFP) and Gaussia luciferase were introduced to MSCs using the same approach.

Animal experiments. All animal experiments were performed in accordance with institutional guidelines approved by the ethical committee from Harvard University. To evaluate the biodistribution of donor cells *in vivo*, MSCs expressing Firefly luciferase were injected either with or without single-cell encapsulation. 3 mg D-luciferin was then injected intraperitoneally into the 25 g mice followed by luminescence imaging with the IVIS Spectrum (PerkinElmer) at indicated times. The systemic secretions of donor cells were evaluated in two ways. For allogeneic transplantation, mMSCs from Balb/c mice expressing Gaussia luciferase were injected into C57/BL6 mice, followed by blood collection at regular time intervals. 10 μl blood was mixed with 100 μl of 20 μg ml^{-1} coelenterazine-h substrate in a white, opaque 96-well plate and luminescence was detected using a BioTek microplate reader. For xenograft, human MSCs encapsulated in either microgels or 250-μm-diameter gels were injected into NOD/SCID/IL-2$\gamma^{-/-}$ mice. For all experiments, each animal was injected with 200,000–300,000 cells. Human MSCs were also encapsulated in either microgels or bulk gel discs and cultured *in vitro*. For each mouse sample, 50 ∼ 100 μl blood plasma was isolated by centrifuging at 2,000 r.p.m. for 15 min and was used to evaluate the systemic level of human IL-6. Both *in vitro* and *in vivo* IL-6 levels were quantified by using an ELISA kit (R&D Systems).